Supplementary Information

Hierarchical 3D Macrosheets Composed of Interconnected In-situ Cobalt Catalyzed Nitrogen doped Carbon Nanotubes as Superior Bifunctional Oxygen Electrocatalysts for Rechargeable Zn-air Batteries

Yapeng Li,[ab] Jingyu Gao,[ab] Fu Zhang,[ab] Qizhu Qian,[ab] Yi Liu,[ab] Genqiang Zhang,*[ab]

[a]*Key Laboratory of Materials for Energy Conversion, Chinese Academy of Science*

[b]*Department of Materials Science and Engineering, University of Science and Technology of China, Hefei, Anhui 230026 China*

*To whom the correspondence should be referred. Email:gqzhangmse@ustc.edu.cn

Webpage: http://zhanglab.ustc.edu.cn/

1. Experimental section

1.1. Materials:

Melamine, oxalic acid, cobalt (II) acetate tetrahydrate ($Co(Ac)_2 \cdot 4H_2O$) and ruthenium dioxide (RuO_2) were purchased from Aladdin Industrial Corporation. 5% Nafion solution was provided by Sigma Aldrich Corporation. 20% Pt/C was provided by Hesen Corporation.

1.2. Synthesis of g-C_3N_4 microsheets

First, bulk g-C_3N_4 is obtained by thermal annealing treatment of melamine in air at 500 ^oC for 2 h. After that, g-C_3N_4 microsheets are then prepared by a simple hydrothermal process. Specifically, 1 g of the bulk g-C_3N_4 was dispersed into 60 ml of oxalic acid aqueous solution (0.5 mM) under stirring, which is then transferred into a 100 mL Teflon-lined stainless steel autoclave and heated at 100 °C for 10 h. Subsequently, after cooled down naturally, the product was obtained by centrifugation, followed by washing with DI water before drying at 60 °C for 12 h.

1.3. Synthesis of g-C_3N_4@Co-glycolate precursor microsheets

In a typical synthesis, 0.2 g of g-C3N4 microsheets are firstly well dispersed into 50 ml of ethylene glycol (EG) dissolved with 0.75 mmol of $Co(CH_3COO)_2 \cdot 4H_2O$ followed by refluxing 170 ^oC for 2 h under stirring. Then, light purple products are collected by repeated washing, centrifugation and drying process. The C/N to Co ratio can be easily adjusted by simply changing the amount of $Co(CH_3COO)_2 \cdot 4H_2O$ during the synthesis while keeping other conditions identical.

1.4. Synthesis of Co@NCNT hierarchical macrosheets (HMS)

The target product of Co@NCNT HMS can be easily obtained by the pyrolysis of the g-C_3N_4@Co-glycolate microsheets in a tube furnace at elevated temperatures ranging from 600 ^oC to 900 ^oC for 4 h with a heating rate of 3 ^oC min^{-1} under Ar atmosphere.

1.5. Characterizations

The morphology and structure of the synthesized materials are characterized by field-emission scanning electron microscopy (FESEM, JSM-6700F), transmission electron microscopy (TEM, JOEL, JEM-2010; Talos F200X), powder X-ray diffractor (XRD, TTR-III,), micropore and chemisorption analyzer (Micrometritics, ASAP 2020) and X-ray photoelectron spectroscopy (XPS, ESCALAB 250).

1.6. Electrochemical measurements

Electrochemical measurements are carried out with a conventional three-electrode system on an electrochemical workstation (CH Instruments 760E) at room temperature. Pt foil (1×1 cm^2) and Ag/AgCl (Saturated KCl)) electrode is used as the auxiliary and reference electrodes, respectively. All potentials in this study were given versus reversible hydrogen electrode (RHE) according the following equation:

$$E(\text{RHE}) = E(\text{Ag/AgCl}) + 0.059\times \text{pH} + 0.198 \quad \text{(S1)}$$

The current density indicated in this work is the apparent current density based on the geometric area of the electrode. A rotating disk electrode (RDE) with glassy carbon (GC) disk electrode (5 mm in diameter) and a rotating ring-disk electrode (RRDE) with a Pt ring (6.5 mm inner diameter and 8.5 mm outer diameter) and a GC disk (5.5 mm diameter) are utilized as the substrate for the working electrodes. Before use, the GC electrodes were carefully polished with 500 and 50 nm Al_2O_3 powders. The catalyst slurries are prepared by dropping 5

mg of catalyst in 1 ml of solution containing 980 µL water/ethanol solution with a volume ratio of 1:1 and 20 µL of 5 wt% Nafion solution (Sigma-aldrich), followed by ultrasonication for 1 h to reach the well dispersion. Then a certain volume of catalyst suspension is casted onto the GC surface to give a 0.28 mg cm^{-2} loading for all samples. For ORR, the loading of 20% Pt/C is 0.1 mg cm^{-2} as the standard loading (0.02 mg_{Pt} cm^{-2}).

1.7. The oxygen reduction reaction (ORR) activity measurements

The cyclic voltammogram (CV) is executed in the Ar/O_2-saturated 0.1 M KOH electrolyte with a scan rate of 50 mV s^{-1}. The linear sweep voltammogram (LSV) tests are conducted by the RDE/RRDE at rotation rates varying from 400 to 2025 rpm in O_2-saturated both 0.1 M and 1 M KOH electrolyte with a scan rate of 5 mV s^{-1}. In order to detect peroxide species formed at the disk electrode, Pt ring electrode in the RRDE measurements is maintained at 1.3 V. The accelerated decay test (ADT) is performed in O_2-saturated 0.1 M KOH at room temperature for 10000 cycles at a scan rate of 100 mV s^{-1} and the polarization curve is then recorded with a sweep rate of 5 mV s^{-1}. The transferred electron number per oxygen molecule (n) involved in ORR was determined by the Koutecky-Levich equation given below:

$$j^{-1}=j_k^{-1} + j_l^{-1}= j_k^{-1}+ B^{-1}\omega^{-1/2} \quad \text{(S2)}$$

Where j, j_k, j_l are the measured current density, the kinetic current and the diffusion-limited current density, respectively. And ω is the angular velocity (rad s^{-1}), B is the Levich slope obtained from the slope of the K-L plots based on the Levich equation as follows:

$$B = 0.62\, nFC_oD_o^{2/3}v^{-1/6} \quad \text{(S3)}$$

Here, n is the number of electrons transferred per oxygen molecule, F is the Faraday constant (F=96485 C mol^{-1}), C_o is the bulk concentration of O_2 (1.2×10^{-6} mol cm^{-3}), D_o is the diffusion

coefficient of O2 in 0.1 M KOH (1.9×10^{-5} cm^2 s^{-1}) and *v* is the kinetic viscosity of the electrolyte (0.01 cm^2 s^{-1}). The transferred electron number (*n*) and H_2O_2 production yield were also calculated according to the formulas as follows:

$$n = 4I_d/(I_d + I_r/N) \quad \text{(S4)}$$

$$H_2O_2\ (\%) = 200\ I_r/(N*I_d)+I_r \quad \text{(S5)}$$

Where I_d is the disk current, I_r is the ring current, *N* is the current collection efficiency (0.37) of the Pt ring and H_2O_2 *(%)* is the production yield during the ORR process.

1.8. The oxygen and hydrogen evolution reaction (OER/HER) activity measurements

All the experiments were executed in the O_2-saturated 1 M KOH aqueous solution. The LSV tests were conducted with GCE (3 mm) at a scan rate of 5 mV s^{-1}. CV experiments were implemented with different scans rate ranging from 10 mV s^{-1} to 100 mV s^{-1}. The chronoamperometric response at the overpotential of 0.32 V is recorded to research the stability. Electrochemical impedance spectroscopy (EIS) was investigated in an O_2-saturated electrolyte with a 5 mV AC potential from 10 kHz to 0.01 Hz. The LSV for HER acitvity is conducted in the Ar-saturated 1 M KOH aqueous solution with GCE (3 mm) at a scan rate of 5 mV s^{-1}.

1.9. The performance of Zn-air battery

The homemade Zn-air battery assembling by zinc plate as the anode, the synthesized Co@NCNT HMS catalysts loaded carbon paper (1 mg cm^{-2}) as the air cathode and a 6.0 M KOH with 0.2 M $Zn(Ac)_2$ as the electrolyte was studied by LSV, EIS and chronopotentiometry to evaluate its performance. The charge and discharge polarization curves are collected on electrochemical workstation (CHI 760E) with the open circuit potential as the initial potential

at the scan rate of 1 mV s^{-1}. The cycling performance of rechargeable Zn-air batteries are conducted on Land-CT2001A at a current density of 5 mA cm^{-2} with periods of 30 min per cycle.

2. Supplementary figures

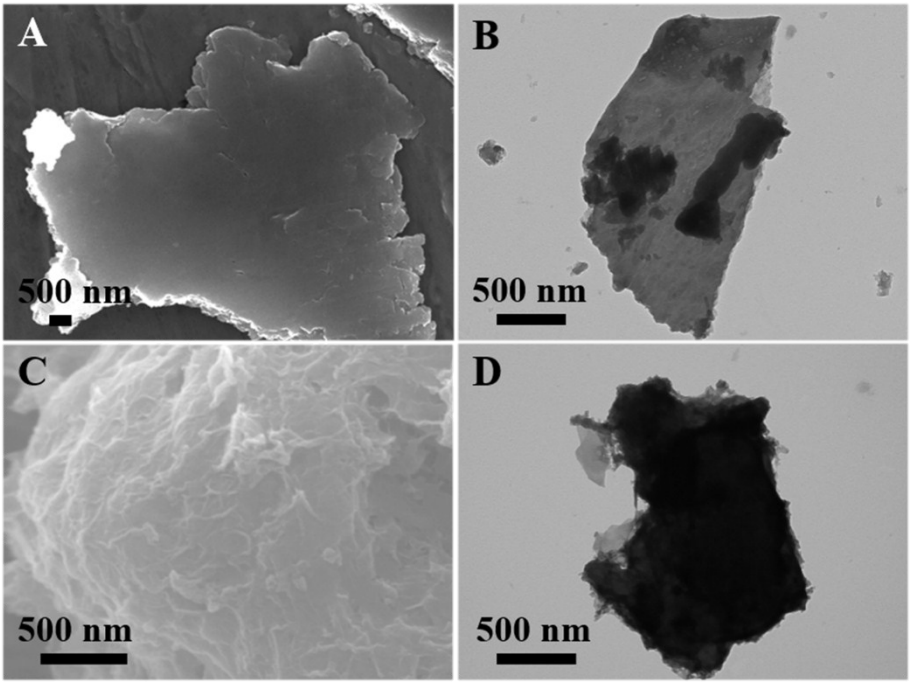

Figure S1. SEM and TEM images of (A, B) g-C_3N_4 microsheets; (C, D) g-C_3N_4@Co-Glycolate composite microsheets.

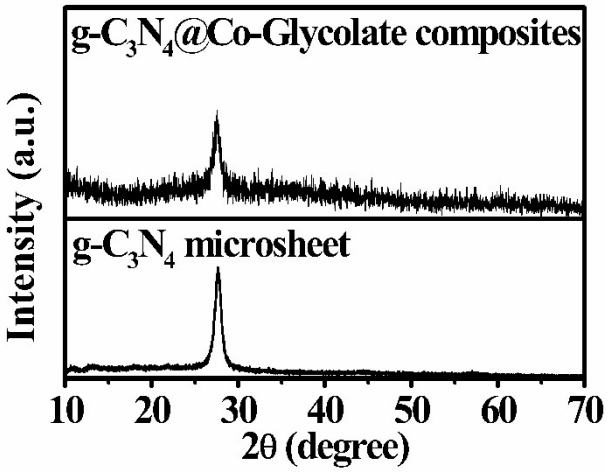

Figure S2. XRD patterns of g-C_3N_4 microsheets and g-C_3N_4@Co-Glycolate composites microsheets.

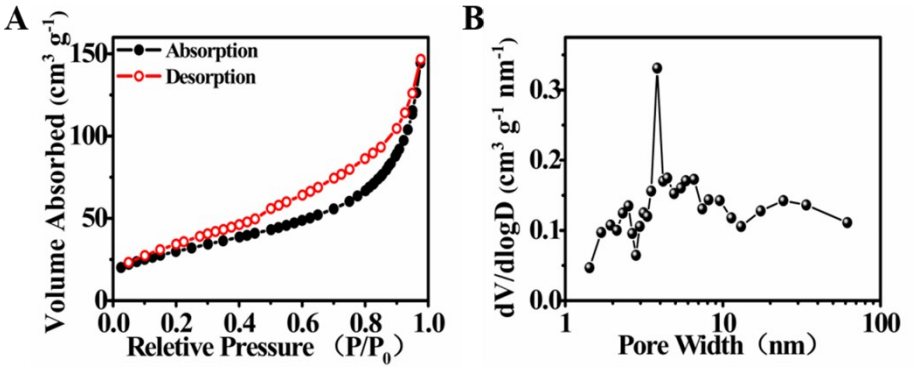

Figure S3. (A) Nitrogen adsorption-desorption isotherms of Co-NCNT HMS synthesized at 600 ^{o}C with 200 mg of g-C_3N_4 microsheets; (B) The corresponding pore size distribution.

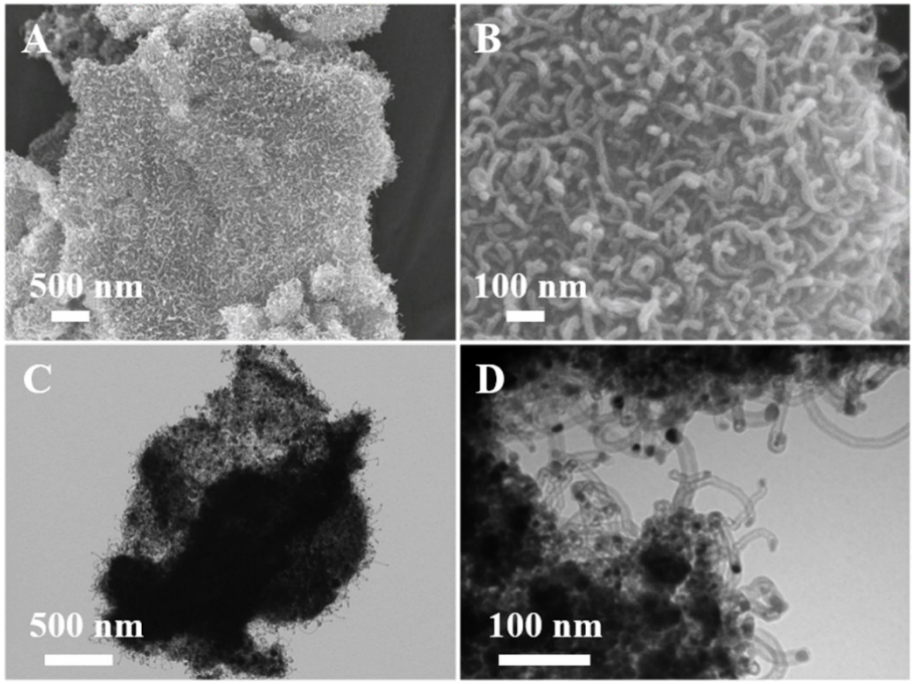

Figure S4. The SEM (A and B) and TEM (C and D) images of Co-NCNT HMS synthesized at 600 ^{o}C with 50 mg of g-C_3N_4 microsheets.

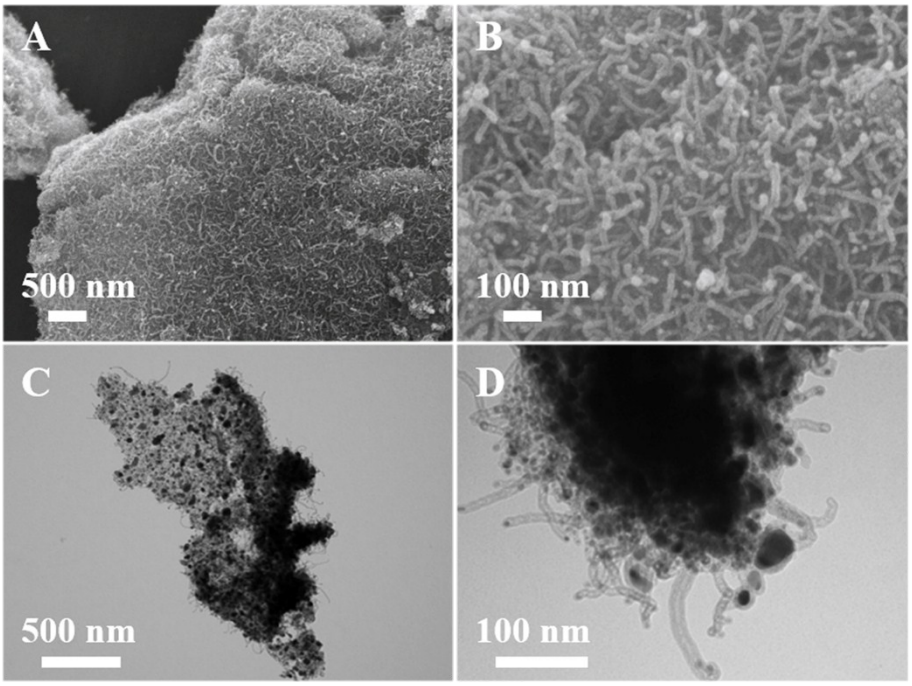

Figure S5. The SEM (A and B) and TEM (C and D) images of Co-NCNT HMS synthesized at 600 ^{o}C with 100 mg of g-C_3N_4 microsheets.

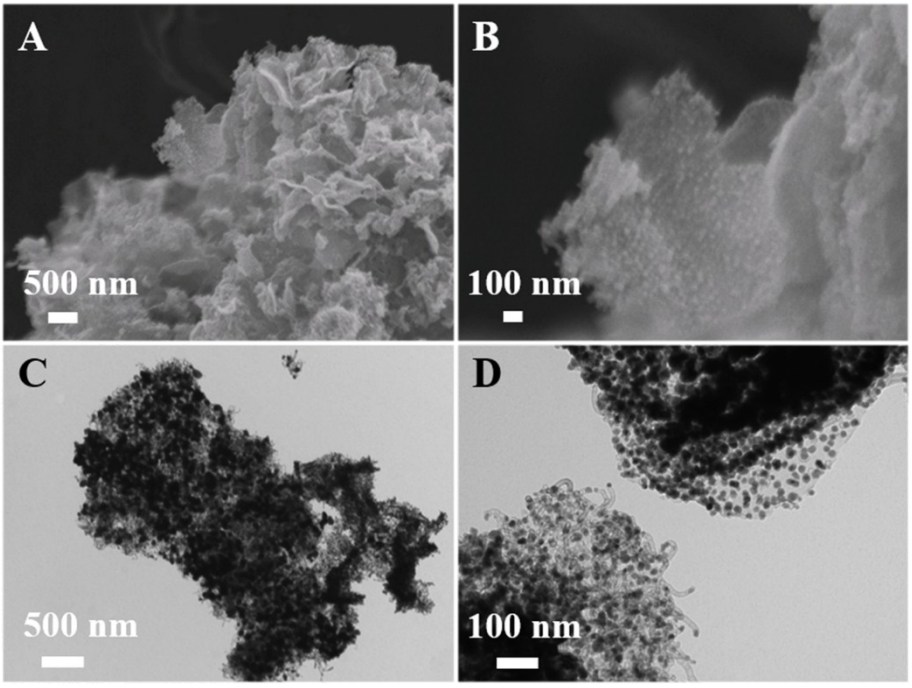

Figure S6. The SEM (A and B) and TEM (C and D) images of Co-NCNT HMS synthesized at 600 ^{o}C with the 300 mg of g-C_3N_4 microsheets.

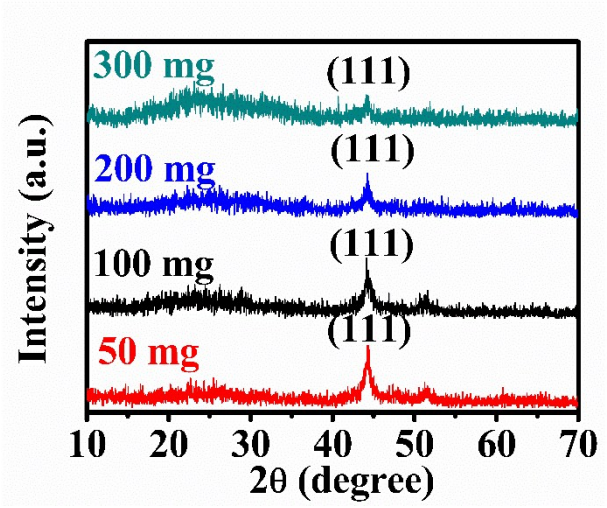

Figure S7. XRD patterns of Co-NCNT HMS synthesized at 600 °C with different amounts of g-C_3N_4 microsheets.

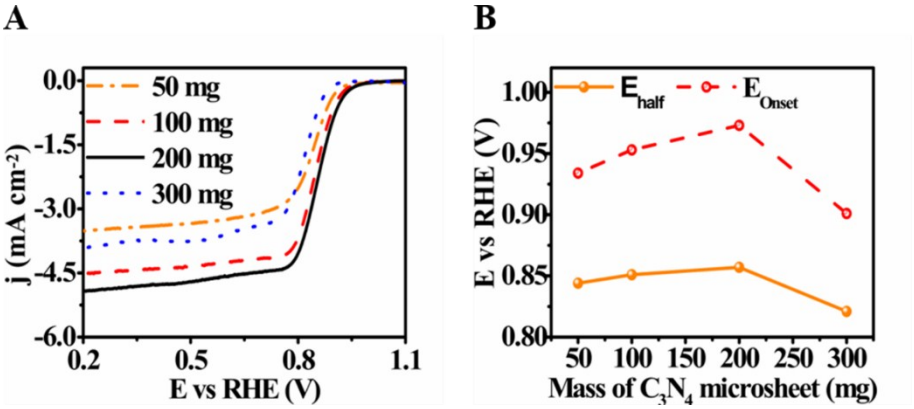

Figure S8. (A) LSV curves of Co-NCNT HMS synthesized at 600 °C with different amounts of g-C_3N_4 microsheets (50 mg, 100 mg, 200 mg and 300 mg) at 1600 rpm in O_2-saturated 0.1 M KOH with a scan rate of 5 mV s^{-1}. (B) The relationship between $E_{1/2}$, E_{onset} and the mass of g-C_3N_4 microsheets.

The influence of microsheets'mass and sintering temperature for ORR were evaluated. The morphologies of Co@NCNT HMS synthesized at 600 ^{o}C with different usage of g-C_3N_4 microsheets (50 mg, 100 mg and 300 mg) were shown in **Figure S4**, **S5** and **S6**. We found that when the usage below 200 mg, the Co@NCNT HMS can be generated and the carbon nanotube array become more sparse along with the increase of g-C_3N_4 microsheet's mass. Nevertheless, the Co anchored carbon microsheet mixed with tiny tubular structure was formed when the mass of g-C_3N_4 microsheet reached 300 mg. This may ascribe to the reduced Co may not catalyze all the g-C_3N_4 microsheet to generate carbon tube. Similarly, the XRD patterns (**Figure S7**) depict that the (111) plane decrease with the increasing dose of g-C_3N_4 microsheet.

The influence of microsheets' mass for ORR were evaluated, firstly. As shown in the **Figure S8A,** the ORR performance of Co@NCNT HMS synthesized at 600 ^{o}C with different usage of g-C_3N_4 microsheets (50 mg, 100 mg, 200 mg and 300 mg) show the following tendency: Co@NCNT HMS (200 mg) > Co@NCNT HMS (100 mg) > Co@NCNT HMS (50 mg) > Co@NCNT HMS (300 mg) The relationship between the E_{half}/E_{onset} of Co@NCNT HMS synthesized at 600 ^{o}C with different usage of g-C_3N_4 microsheets (50 mg, 100 mg, 200 mg and 300 mg) and the mass of g-C_3N_4 microsheets were presented in the **Figure S8B**. The more positive $E_{1/2}$ and E_{onset} of Co@NCNT HMS may due to the sparse structure accelerate diffusion of active specie and the more accessible active site of Co-N_x improve the chance of oxygen reduction.

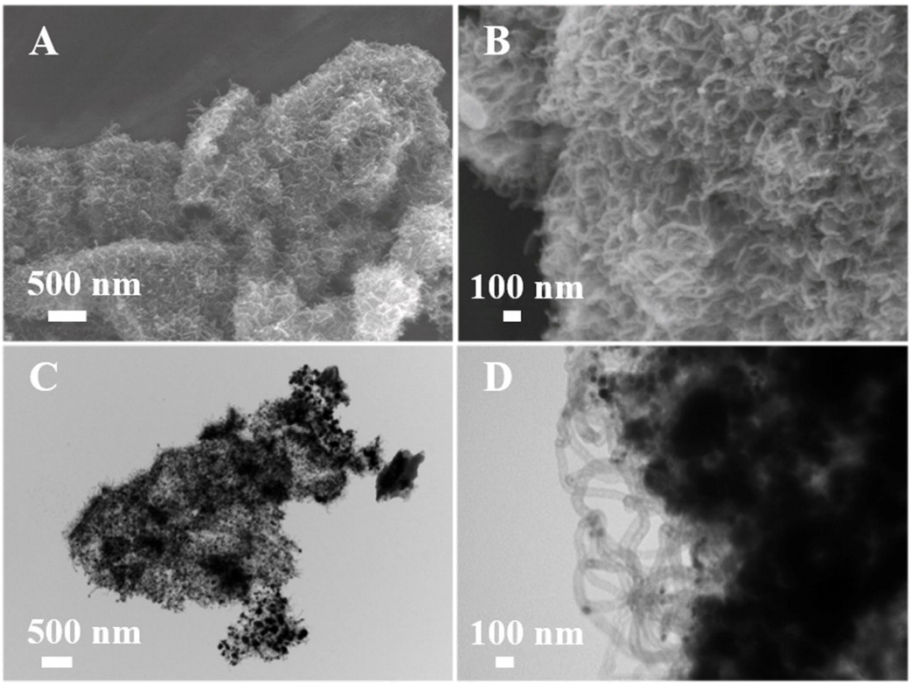

Figure S9. The SEM (A and B) and TEM (C and D) images of Co-NCNT HMS synthesized at 700 ^{o}C with 200 mg of g-C_3N_4 microsheets.

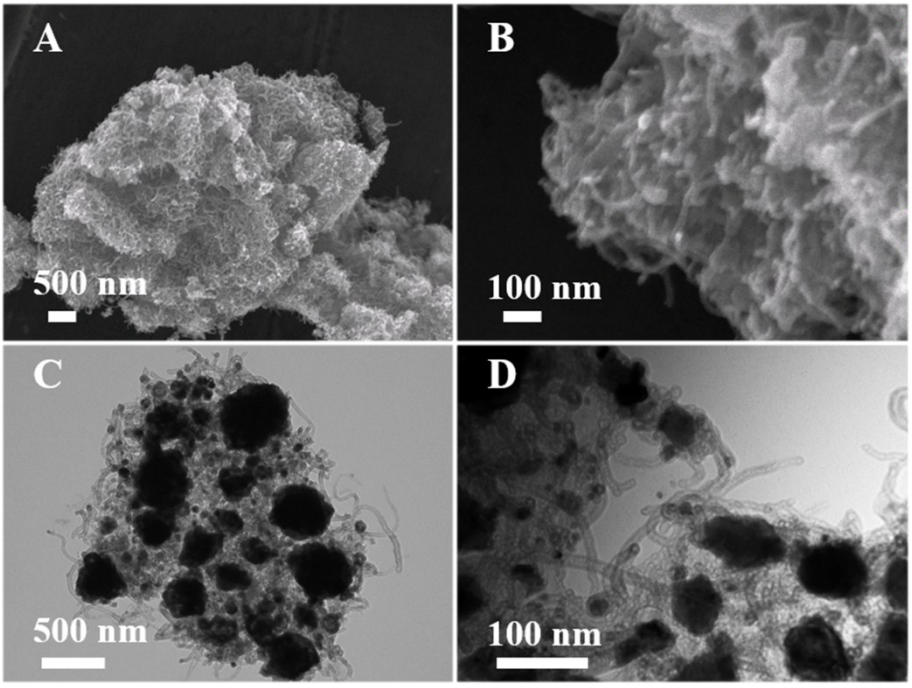

Figure S10. The SEM (A and B) and TEM (C and D) images of Co-NCNT HMS synthesized at 800 ^{o}C with 200 mg of g-C_3N_4 microsheets.

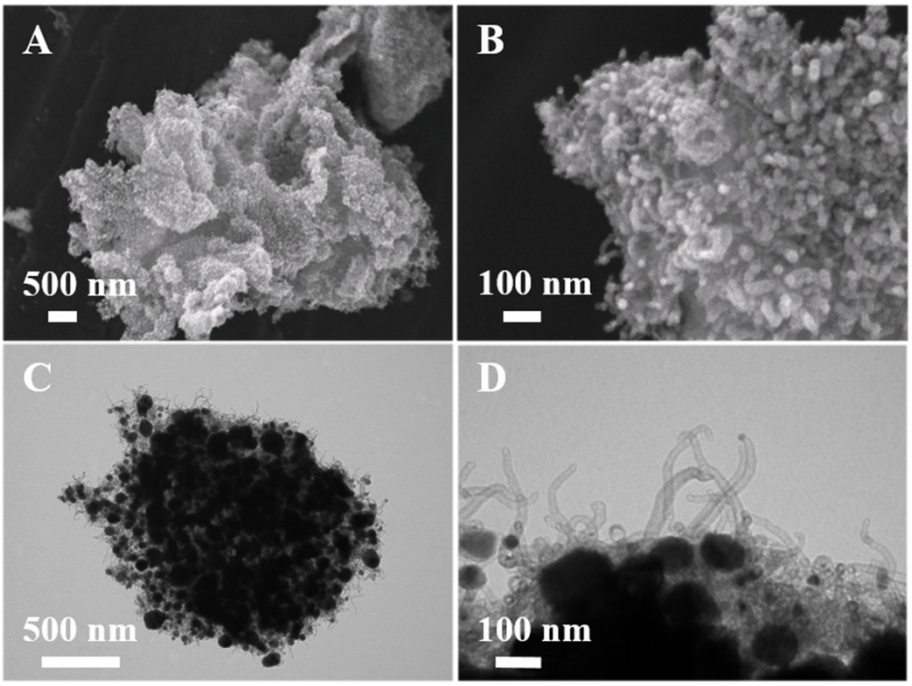

Figure S11. The SEM (A and B) and TEM (C and D) images of Co-NCNT HMS synthesized at 900 ^{o}C with 200 mg of g-C_3N_4 microsheets.

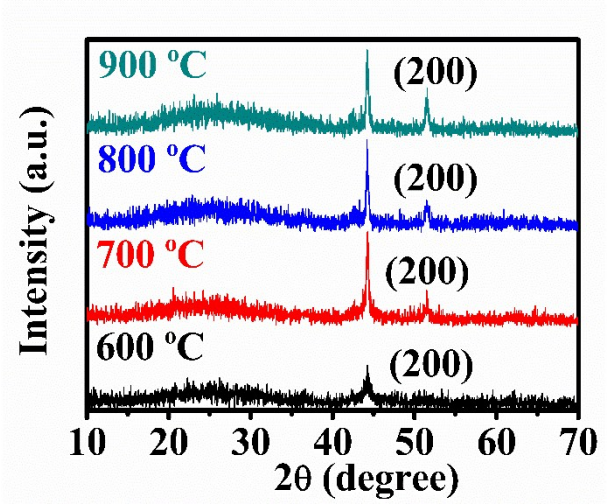

Figure S12. XRD patterns of Co-NCNT HMS synthesized at different sintering temprature (600 ^{o}C, 700 ^{o}C, 800 ^{o}C and 900 ^{o}C) with 200 mg of g-C_3N_4 microsheets.

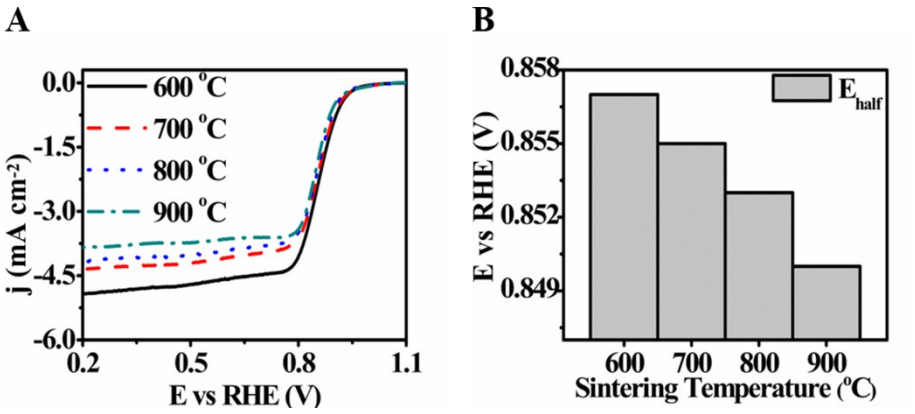

Figure S13. (A) LSV curves of Co-NCNT HMS synthesized at different sintering temprature (600 °C, 700 °C, 800 °C and 900 °C) with 200 mg of g-C_3N_4 microsheets at 1600 rpm in O_2-saturated 0.1 M KOH with a scan rate of 5 mV s^{-1}. (B) The relationship between E_{half} and the sintering temperature.

Then, the sintering temperature (600 °C, 700 °C, 800 °C and 900 °C) may influence the morphology and crystallinity of Co@NCNT HMS with 200 mg of g-C_3N_4 microsheets. Increasing the temperature, the Co nanocluster on the surface of nanotube may immigrate, agglomerate and form bigger agglutination; the nanotube may convergence and block the active site (**Figure S9, S10 and S11**).[1] Also, the more narrow and intense peak of cobalt's (002) crystal plane along with the higher pyrolysis temperature imply the bigger particle size of Co nanocluster, which is in accordance with the morphology characterization (**Figure S12**).[2] The LSV plots in **Figure S13A** depicts the ORR performance of Co@NCNT HMS synthesized at different sintering temperature (600 °C, 700 °C, 800 °C and 900 °C) with 200 mg of g-C_3N_4 microsheets. Results depict that along with the higher temperature, the polarization curves shift negatively and the current platform shift positively. This may be relevant to the lower defect density generated as a result of the higher pyrolysis temperature.[3, 4] Moreover, the residual metallic Co nanoparticles encapsulated by carbon shells are also believed to play an important role in the excellent electrocatalytic activity and the agglomerate of Co nanocluster along with the increasing temperature may reduce the available content of Co.[5]

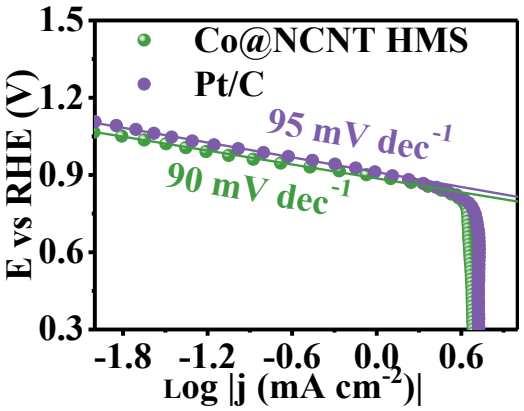

Figure S14. The corresponding Tafel plots of Co@NCNT HMS and Pt/C, which were calculated from Figure 4B.

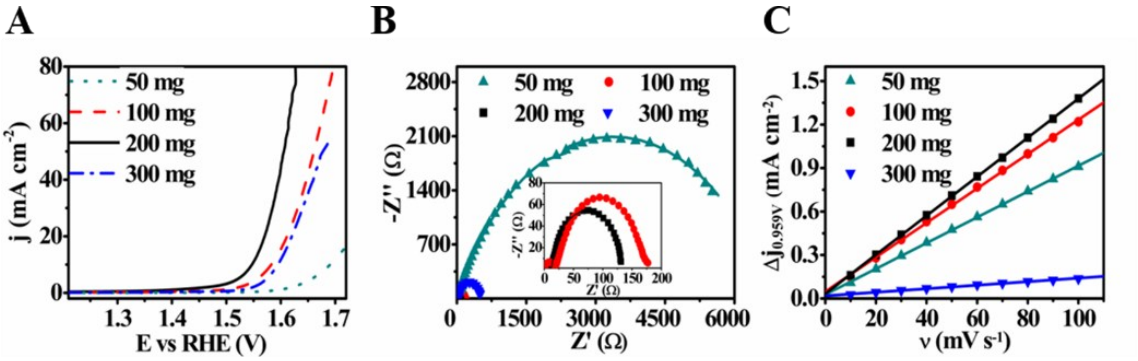

Figure S15. (A) Polarization curves of Co-NCNT HMS synthesized at 600 °C with different amounts of g-C_3N_4 microsheets in 1 M KOH with a scan rate of 5 mV s^{-1}; (B) The corresponding Nyquist plots at overpotential of 300 mV. The inset is the enlarged plot; (C) The capacitive current density at 0.959 V (vs. RHE) as a function of scan rate.

Figure S15A depicts that with the increasing mass of g-C_3N_4, the capacity of Co@NCNT HMS synthesized at 600 °C (50 mg, 100 mg, 200 mg, 300 mg) become better and 200 mg is the optimal mass to reach the best catalytic activity, then the inferior activity appears along with the increasing dosage (300 mg) of g-C_3N_4 microsheet. Similarly, the tendency of R_{ct} and C_{dl} with the increase of g-C_3N_4 microsheets' content emerge the volcano behavior (**Figure S15B and C**). Hence, the Co@NCNT HMS exhibits the best OER performance among all the Co-NCNT

HMS synthesized at 600 ^{o}C with different usage of g-C_3N_4 microsheets (50 mg, 100 mg, 200 mg and 300 mg). The smallest R_{ct} (125.3 Ω) and biggest C_{dl} (6.73 mF cm^{-2}) may explain its better activity. The synergistic effect between the appropriate content of graphitic nitrogen, Co-N_x and Co may optimize the performance of Co@NCNT HMS.[6, 7] In addition, the 3D network assembled by 1D tube expose more active site and profit the absorption and dissociation of oxygen.

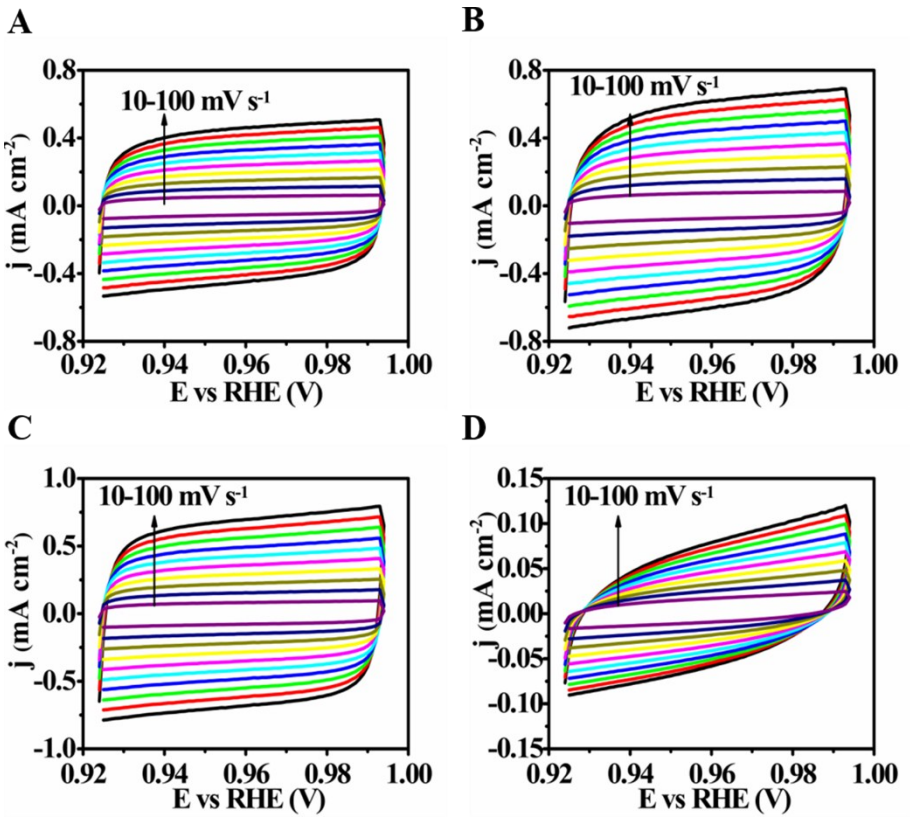

Figure S16. Cyclic voltammograms of Co-NCNT HMS synthesized at 600 ^{o}C with 50 mg (A), 100 mg (B), 200 mg (C) and 300 mg (D) of g-C_3N_4 microsheets at scan rates from 10 to 100 mV s^{-1}

From cyclic voltammogram in **Figure S16,** the electrochemically active surface areas (ECSA) of them can be estimated from the electrochemical double-layer capacitance (C_{dl}) by collecting cyclic voltammograms in a non-Faradaic region of 0.924 - 0.994 V vs RHE (**Figures S16 A, B and C**).[8, 9] It is widely accepted that the ECSA of a material is proportional to its C_{dl} value, which can be derived from the linear slope of its current density versus scan rate.[10] The calculated C_{dl} value of the Co@NCNT HMS synthesized at 600 ^{o}C with 200 mg of g-C_3N_4 microsheets is about 6.73 mF cm^{-2} and much higher than that of Co@NCNT HMS synthesized at 600 ^{o}C with 50 mg of g-C_3N_4 microsheets (4.44 mF cm^{-2}), 100 mg of g-C_3N_4 microsheets (5.93 mF cm^{-2}) and 300 mg of g-C_3N_4 microsheets (0.61 mF cm^{-2}). The high ECSA value renders a large functioning surface area of its catalytically active sites, excellent gas bubble removal ability, and thus superior catalytic performance.[11]

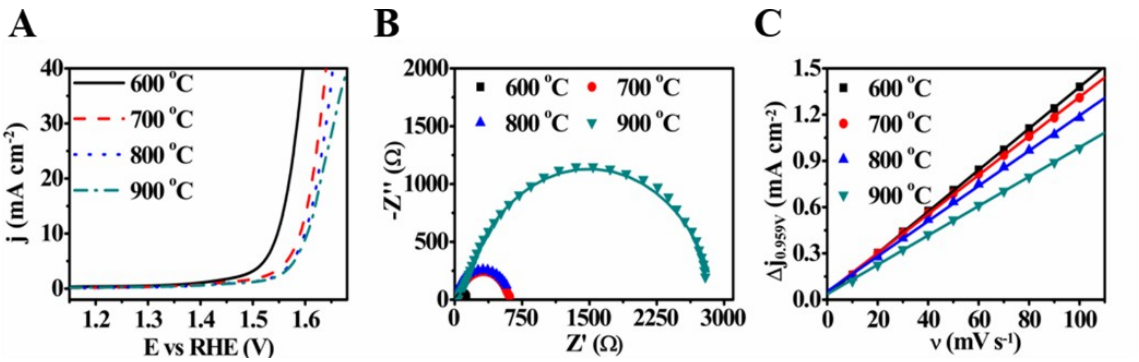

Figure S17. (A) Polarization curves of LSV curves of Co-NCNT HMS with different temperatures with 200 mg of g-C_3N_4 microsheets in 1 M KOH with a scan rate of 5 mV s^{-1}; (B) The corresponding Nyquist plots at overpotential of 300 mV; (C) The capacitive current density at 0.959 V (vs. RHE) as a function of scan rate for Co-NCNT HMS synthesized at different sintering temprature (600 °C, 700 °C, 800 °C and 900 °C) with 200 mg of g-C_3N_4 microsheets.

Pyrolysis temperature also influences the OER performance. **Figure S17A** depicts that with the raise of temperature, the capacity of Co@NCNT HMS synthesized at higher temperature (> 600 °C) with 200 mg of g-C_3N_4 microsheets become worse. Similarly, bigger R_{ct} and smaller C_{dl} along with the increase temperature further indicate the worse performance for OER (**Figure S17B and C**). Hence, the Co@NCNT HMS, which show smallest R_{ct} (125.3 Ω) and biggest C_{dl} (6.73 mF cm^{-2}), possesses the best OER performance among all the Co-NCNT HMS synthesized at different sintering temperature (600 °C, 700 °C, 800 °C and 900 °C) with 200 mg of g-C_3N_4 microsheets. Aggregated Co nanocluster and fused carbon nanotube may result in the subsequence.[1]

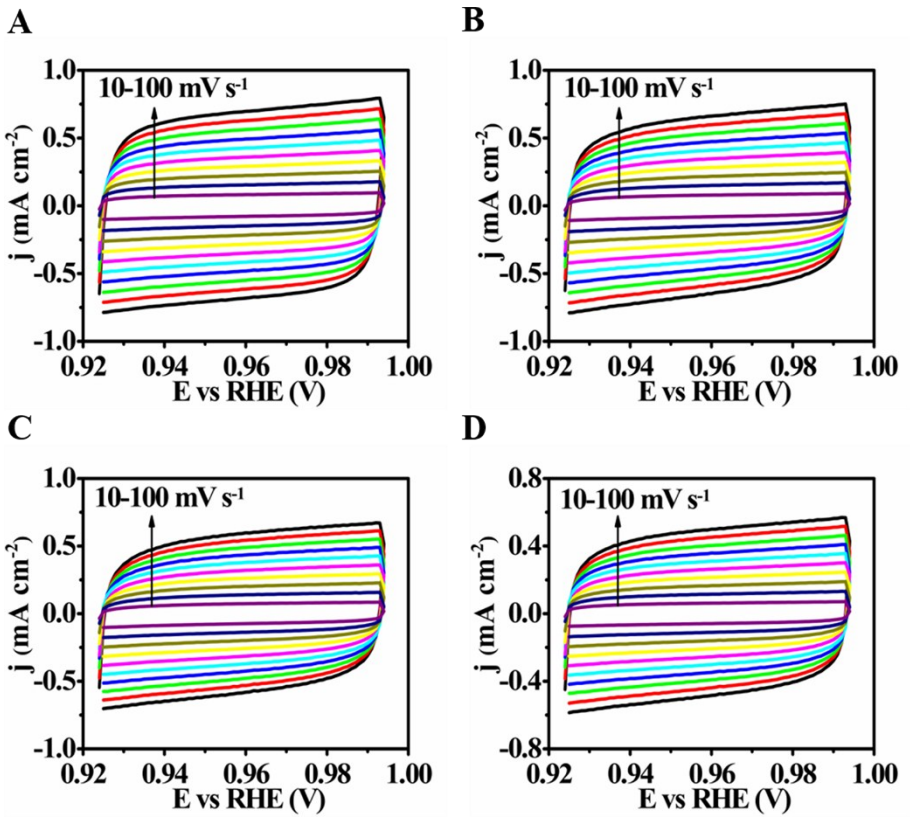

Figure S18. Cyclic voltammograms of Co-NCNT HMS synthesized at 600 °C (A), 700 °C (B), 800 °C (C) and 900 °C (D) with 200 mg of g-C_3N_4 microsheets at scan rates from 10 to 100 mV s^{-1}.

The cyclic voltammograms which were collected in a non-Faradaic region and the corresponding linear extrapolation graphs indicate that Co@NCNT HMS synthesized at 600 °C with 200 mg of g-C_3N_4 microsheets has the biggest ECSA value (6.73 mF cm^{-2}) compared with Co@NCNT HMS synthesized at 700 °C (6.33 mF cm^{-2}), Co@NCNT HMS synthesized at 800 °C (5.71 mF cm^{-2}) and Co@NCNT HMS synthesized at 900 °C (4.76 mF cm^{-2}) with 200 mg of g-C_3N_4 microsheets.

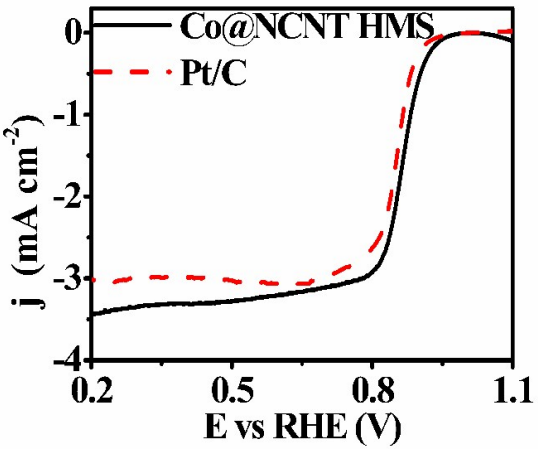

Figure S19. LSV curves of Co@NCNT HMS and commercial E-TEK Pt/C at 1600 rpm in O_2-saturated 1 M KOH with a scan rate of 5 mV s^{-1}.

We also investigate the ORR capacity of Co@NCNT HMS in O_2-saturated 1 M KOH. **Figure S22** picture that the Co@NCNT HMS manifest better performance for ORR in both onset overpotential and half-wave potential (Co@NCNT HMS: E_{onset}=0.950 V, $E_{1/2}$=0.868 V; 20 % Pt/C: E_{onset}=0.926 V, $E_{1/2}$=0.850 V) when measured in 1M KOH electrolyte.

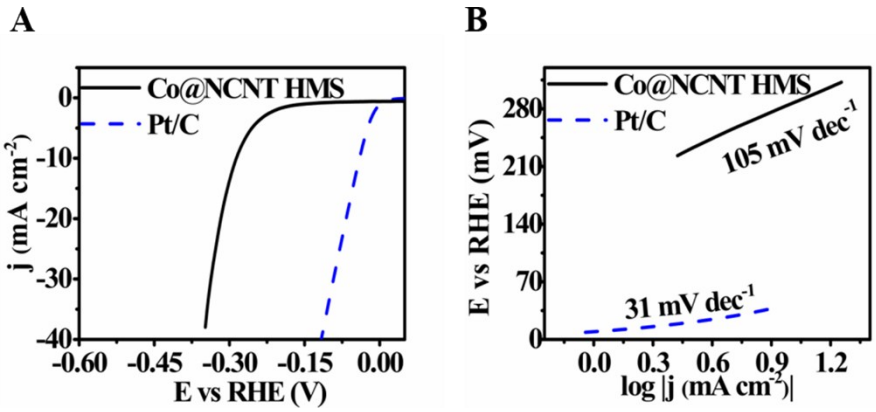

Figure S20. (A) Polarization curves of Co@NCNT HMS and 20 % Pt/C in 1 M KOH with a scan rate of 5 mV s^{-1}. (B) The corresponding Tafel plots.

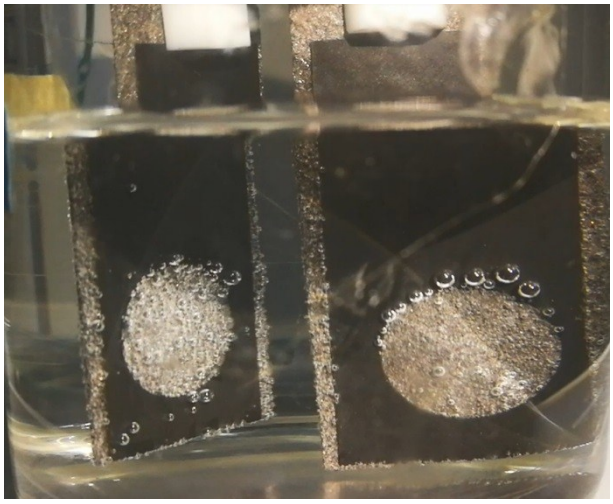

Figure S21. The digital photograph of Co@NCNT HMS as anode and cathode of overall water-splitting powered by two homemade Zn–air batteries connected in series with Co@NCNT HMS as the air cathode.

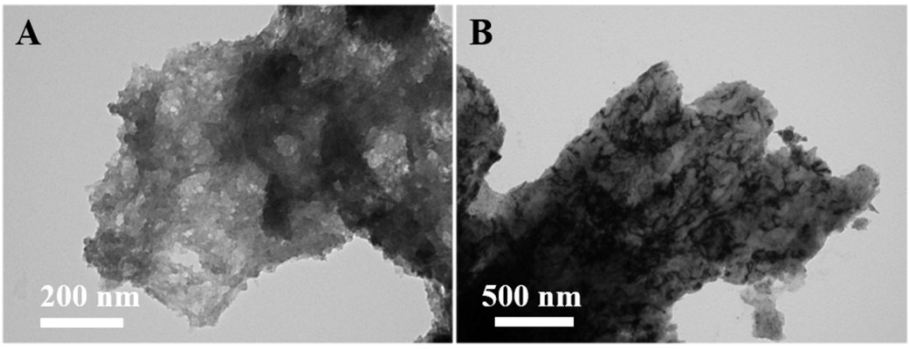

Figure S22. The TEM images of (A) N-Carbon and (B) Co-Carbon obtained by sintering g-C_3N_4 microsheets and Co-Glycolate composite microsheets at 600 ^oC under Ar atmosphere.

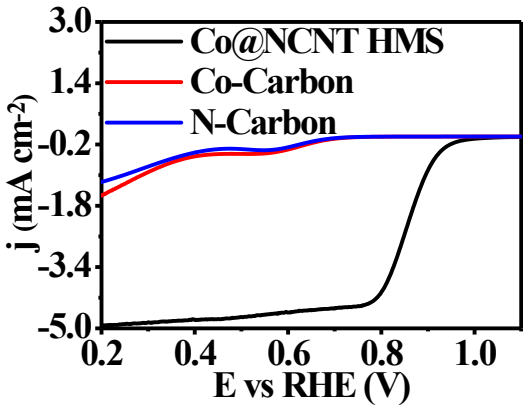

Figure S23. (A) Polarization curves of Co@NCNT HMS, Co-Carbon and N-Carbon in 0.1 M KOH with a scan rate of 5 mV s^{-1}.

The inferior ORR activity of Co-Carbon and N-Carbon may shed light on that the existence of Co-Nx is important for the improved ORR activity. Also, the random morphology of Co-Carbon and N-Carbon and the worse reactivity of them may further suggest the well-defined macrosheets composed by the interconnected nanotubes is beneficial for the ameliorating of ORR activity.

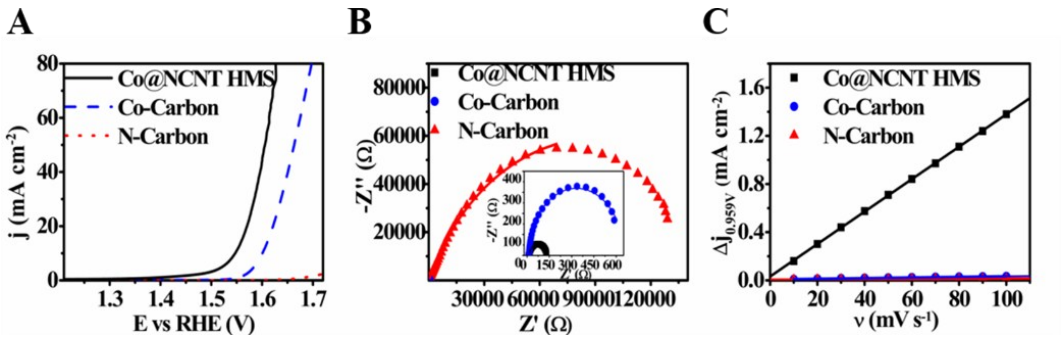

Figure S24. (A) Polarization curves of Co@NCNT HMS, Co-Carbon and N-Carbon in 1 M KOH with a scan rate of 5 mV s^{-1}. (B) The corresponding Nyquist plots of Co@NCNT HMS, Co-Carbon and N-Carbon at overpotential of 300 mV. (C) The capacitive current density at 0.959 V (vs. RHE) as a function of scan rate for Co@NCNT HMS, Co-Carbon and N-Carbon.

The poor OER performance of N-carbon may ascribe to the huge charge transfer resistance (Rct = 180710 Ω) and small electrochemically active area (C_{dl} = 0.054 mF cm^{-2}). This may due to the incomplete pyrolysis of g-C_3N_4 microsheets without the help of Co species at 600 ^oC. And, the Co-Carbon needs the overpotential of 370 mV to reach the current density of 10 mA cm^{-2}. The bigger Rct (498.9 Ω) may result in the absence of carbon tube and the smaller C_{dl} (0.13 mF cm^{-2}) may attribute to the random structure with more aggregated Co nanocluster and the deficiency of active Co-N_x or graphitic nitrogen.[12] This also imply Co may has more important role on OER.[13]

Table S1. The bifunctional activity of different catalysts for ORR and OER

Catalyst	$\Delta E_{(Ej10-E1/2)}$ (mV)	reference
NC-Co_3O_4/CC	718	*Adv. Mater.* **2017**, *29*, 1704117
Co_3O_4/NVC	911*	RSC Adv., 2015, 5, 75773–75780
CoO-Co/CNF	809	J. Power Sources *2017, 364*, 101-109.
CoO/SnO_2/NG-500	720	RSC Adv., 2016 *6*, 50017
FeCo-Co 4 N/N-C FeCo-Co_4N/N-C	750	Adv. Mater.*, 2017, 29,* 1704091.
Co_4N/CNW/CC	740	J. Am. Chem. Soc., 2016 *138*, 10226
$Fe_{0.5}Co_{0.5}$Ox/NrGO	740*	Adv. Mater., 2017, *29*, 1701410.
NC@Co-NGC DSNC	820*	Adv. Mater., 2017 *29*, 1700874.
$Co(OH)_2$+N-rGO	870	ACS Appl. Mater. Inter, 2015 *7*, 12930
CuCoOx/FeOOH	720	ACS Energy Letters, 2017, *2*, 2498-2505
Co@NCNT HMS	681	This work
Pt/C+RuO_2	714	This work

*means the electrolyte is 0.1 M KOH.

3. Supplementary references

1 C. Wei, H. Wang, K. Eid, J. Kim, J. H. Kim, Z. A. Alothman, Y. Yamauchi and L. Wang, *Chem. Eur. J.*, 2017, **23**, 637-643.

2 C. Wang, D. van der Vliet, K.-C. Chang, H. You, D. Strmcnik, J. A. Schlueter, N. M. Markovic and V. R. Stamenkovic, *J. Phys. Chem. C*, 2009, **113**, 19365-19368.

3 B. Y. Xia, Y. Yan, N. Li, H. B. Wu, X. W. Lou and X. Wang, *Nat. Energy*, 2016, **1**, 15006.

4 X. Zou, X. Huang, A. Goswami, R. Silva, B. R. Sathe, E. Mikmekova and T. Asefa, *Angew. Chem., Int. Ed.*, 2014, **53**, 4372-4376.

5 L. Wang, A. Ambrosi and M. Pumera, *Angew. Chem., Int. Ed.*, 2013, **52**, 13818-13821.

6 Y. Zhao, R. Nakamura, K. Kamiya, S. Nakanishi and K. Hashimoto, *Nat. Commun.*, 2013, **4**, 2390.

7 P. Chen, K. Xu, Z. Fang, Y. Tong, J. Wu, X. Lu, X. Peng, H. Ding, C. Wu and Y. Xie, *Angew. Chem., Int. Ed.*, 2015, **54**, 14710-14714.

8 N. Jiang, B. You, M. Sheng and Y. Sun, *Angew. Chem., In.t Ed.*, 2015, **54**, 6251-6254.

9 X. Y. Lu and C. A. Zhao, *Nat. Commun.*, 2015, **6**.

10 F. Song and X. Hu, *Nat. Commun.*, 2014, **5**.

11 B. You, N. Jiang, M. Sheng, M. W. Bhushan and Y. Sun, *ACS Catal.*, 2015, **6**, 714-721.

12 S. Gadipelli, T. Zhao, S. A. Shevlin and Z. Guo, *Energy Environ. Sci.*, 2016, **9**, 1661-1667.

13 X. Zhang, R. Liu, Y. Zang, G. Liu, G. Wang, Y. Zhang, H. Zhang and H. Zhao, *Chem. Commun.*, 2016, **52**, 5946-5949.